

MRI Scan Synthesis Methods based on Clustering and Pix2Pix

Giulia Baldini^{*†}Melanie Schmidt^{*‡}Charlotte Zäske[§]Liliana L. Caldeira[¶]

May 6, 2024

We consider a missing data problem in the context of automatic segmentation methods for Magnetic Resonance Imaging (MRI) brain scans. Usually, automated MRI scan segmentation is based on multiple scans (e.g., T1-weighted, T2-weighted, T1CE, FLAIR). However, quite often a scan is blurry, missing or otherwise unusable. We investigate the question whether a missing scan can be synthesized. We exemplify that this is in principle possible by synthesizing a T2-weighted scan from a given T1-weighted scan.

Our first aim is to compute a picture that resembles the missing scan closely, measured by *average mean squared error* (MSE). We develop/use several methods for this, including a random baseline approach, a clustering-based method and pixel-to-pixel translation method by Isola et al. [14] (Pix2Pix) which is based on conditional GANs. The lowest MSE is achieved by our clustering-based method.

Our second aim is to compare the methods with respect to the effect that using the synthesized scan has on the segmentation process. For this, we use a DeepMedic model trained with the four input scan modalities named above. We replace the T2-weighted scan by the synthesized picture and evaluate the segmentations with respect to the tumor identification, using Dice scores as numerical evaluation. The evaluation shows that the segmentation works well with synthesized scans (in particular, with Pix2Pix methods) in many cases.

1 Introduction

Automated brain tumor segmentation is an active and highly relevant research field [25, 29, 37] with its own annual data challenge called BraTS (*Brain Tumor Segmentation Challenge*). Given a set of MRI scans, the objective of automated tumor segmentation is to find and segment a tumor in the depicted brain automatically. Segmentation software (e.g., DeepMedic [16], nnU-Net [13]) is not only able to find the exact tumor location, but also to distinguish between different subregions of the tumor, such as edema and necrosis. These methods [13, 16] use a set of four modalities to achieve this purpose, namely T1W (T1-weighted), T2W (T2-weighted), T1CE (T1-weighted contrast enhanced) and FLAIR. However, in the clinical routine, it is uncommon that all modalities are available for a single examination.

^{*}This work was partly funded by DFG, project numbers 416767905 and 456558332.

[†]G. Baldini (giulia.baldini@hhu.de) is affiliated with the Department of Computer Science, Heinrich-Heine-University Düsseldorf, Universitätsstraße 1, 40225, Düsseldorf, Germany.

[‡]M. Schmidt (mschmidt@hhu.de) is affiliated with the Department of Computer Science, Heinrich-Heine-University Düsseldorf, Universitätsstraße 1, 40225, Düsseldorf, Germany.

[§]C. Zäske (charlotte.zaeske@rwth-aachen.de) is affiliated with the Department of Diagnostic and Interventional Radiology, University Hospital Aachen, Pauwelsstraße 30, 52074, Aachen, Germany

[¶]L. L. Caldeira (liliana.caldeira@uk-koeln.de) is affiliated with the Department of Radiology, University Hospital of Cologne, Kerpener Str. 62, 50937, Cologne, Germany.

^{||}L. L. Caldeira and M. Schmidt have jointly supervised this project.

While it is plausible to create separate networks for each subset of available scans, a more convenient approach is to address the missing data directly and replace the missing scan. Indeed, a recent BraTS challenge [18] states that *the ability to substitute missing modalities and gain segmentation performance is highly desirable and necessary for the broader adoption of these algorithms in the clinical routine.*¹ We showcase that creating synthesized scans is possible to a certain extent by investigating the following question:

How can we produce a reasonable synthesized T2W image from a T1W scan of the same patient?

Figure 1 shows a slice of a T1W scan and the corresponding slice of the T2W scan of the same patient (these scans are 3D, but we only depict one slice). Since T2W looks complementary to T1W, a first idea might be to inverse every voxel, i.e., to transform the voxel intensity p_{T1W} of T1W to $p_{T2W} = \min(T1W) + \max(T1W) - p_{T1W}$ where $\min(T1W)$ and $\max(T1W)$ are the minimum and maximum values of all voxels in T1W. This transformation is what created the third picture in Figure 1. Our goal is to substantially beat this baseline approach.

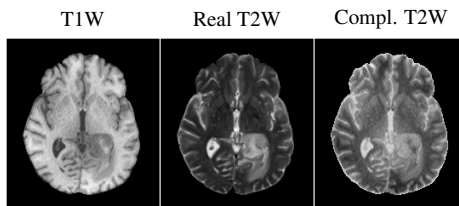


Figure 1: A slice of a T1W and a T2W scan, and of the T1W complement (Patient BraTS19 CBICA BLI 1).

We develop and evaluate two methods. The first one is based on clustering. It uses a training data set to understand the relationship between T1W and T2W. For a set of given T1W and T2W scans, the method learns the intensity spectrum of each tissue in T1W and how it is translated into the corresponding spectrum that the tissue has in T2W. This is done by identifying areas of similar color in both pictures via clustering, and then mapping compatible areas to each other in order to compute a color transformation table. While clustering methods have been applied in medical imaging, the primary focus has been on aiding brain tissue segmentation [8, 9, 19, 20, 23]. Our BrainClustering approach is conceptually different from other works in the area and might lead to further work on related problems. We describe our clustering method in detail in Section 2. The second method is an application of a known tool named Pix2Pix [14, 34] that has already been used in a variety of medical applications for image-to-image translation [1, 4, 11, 38]. We use it with slight modifications of the software that we describe in Section 3. In follow-up work, Raut et al. [30] uses this same modified version of Pix2Pix to generate and evaluate different mappings (e.g., T2W to FLAIR).

Our evaluation is based on a data set based on 460 patients from BraTS 19 [2, 3, 21]. We both evaluate how close the synthesized picture is to the true scan with respect to minimum mean squared error (MSE) as well as how using it affects the segmentation process. For 335 patients, the BraTS 19 data is supplemented with a ground truth segmentation. A radiologist segmented the scans for 15 additional patients to increase the number of cases with ground truth. 110 cases remain that have no ground truth.

2 BrainClustering

We name our clustering algorithm BrainClustering. It computes a synthesized T2W image by applying a chain of several clustering and mapping steps. The clusterings are used to build mapping tables, and these tables are in turn used to generate a synthesized T2W. We refer to the process of building these mapping tables as *training*, even though it does not involve a neural network model. The following training steps are applied to pairs of given T1W and T2W which we process to understand how to

¹Note, however, that our work was mostly done before that challenge was posed, so in particular, we are using the BraTS 2019 data set for our experiments.

construct a T2W image from a T1W image. Figure 2 gives an overview of the process for a single patient, i.e., for one pair of T1W and T2W.

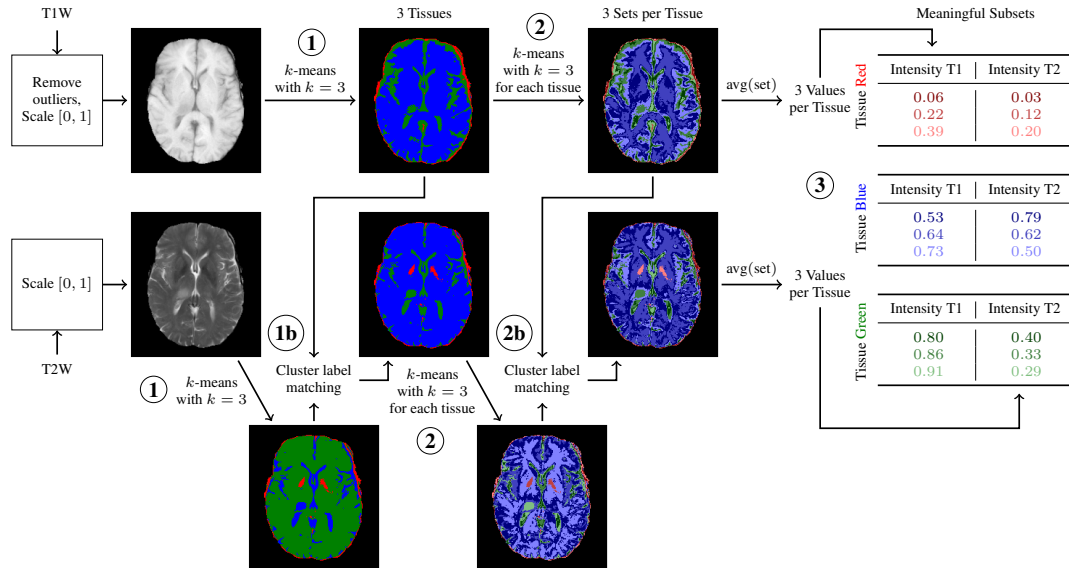


Figure 2: [Best viewed in color] Schematic representation of the BrainClustering process: First, we use k -means1d to obtain a macro clustering of the scan according to the desired number of macro clusters. Second, each macro cluster is clustered into micro clusters. Finally, the points belonging to these micro clusters are averaged and stored in one table for each tissue, where there is an entry for each corresponding value of T1W and T2W.

Training Step 1: Both images are segmented into *macro clusters*. The segmentation is done by solving a one-dimensional k -means problem optimally by dynamic programming with the implementation k -means1d [10, 33, 36]. In the example, the number of macro clusters k is 3. Since the macro clusters are supposed to correspond to the different tissues, they should intuitively be equal to the number of different tissues. However, the process works better if we allow a little more macro clusters to account for varieties of tissues. Empirically, a good range is between three and six clusters.

Training Step 1b: As an intermediate step after finding the macro clusters, we need to identify which cluster represents what tissue. The tissues in T1W can be identified by ordering the clusters according to the average intensity value of their pixels. We could do a similar approach to finding the tissues in T2W, but we instead find them by matching them to the found clusters in T1W as described below in Step 2b (cluster label matching).

Training Step 2: Next, we compute a *micro clustering* for each tissue which captures the shadings of the tissues and the relation between the shading in T1W and T2W. We again implement this step by optimally solving a one-dimensional k -means problem. The number of micro clusters corresponds to the number of different shades that we allow. In Figure 2, we use 3 micro clusters per tissue for visualization purposes, while in practice, we use at least 100 micro clusters.

Training Step 2b: Now, there are micro clusters for every tissue, both in T1W and in T2W. They are small patches of the same shading, and we aim to identify how such a patch in T1W is mapped to T2W. For this, we need to match the clusters in T1W and T2W. We call this process *cluster label matching*. The matching is done by first excluding voxels that are only present in one of the scans (since the scans are registered to the same template, these are only a few voxels), and then finding the label that maximizes the number of voxels that the matched clusters have in common. The problem reduces to maximum weighted matching problem, which we solve with the Hungarian method [15].

After this step, we have a macro clustering and every macro clustering is subdivided into small patches, and every small patch in T1W has its specified counterpart in T2W.

Training Step 3: The next step is to capture the relationship between the shadings in T1W and T2W. The idea behind this is that we assume that it is possible to map the shading of a specific tissue in T1W to the shading of the same tissue in T2W. We model this by using a function f_t for every tissue

which is supposed to translate intensity values from T1W to intensity values in T2W. We later want to use the function $f_t(i_1) = i_2$ to predict the T2W intensities of a patient whose T2W scan is missing.

For every tissue type t , we have computed a micro clustering and matched the micro clusters between the two scans. Now we compute the average of the points in each micro cluster of T1W, which we call a_1 . Then, we compute the average for each corresponding micro cluster of T2W, which we call a_2 . Finally, we add a new entry (a_1, a_2) to f_t , which is the map corresponding to the current macro cluster/tissue type. It may happen that there already is an entry with key a_1 stored in the map. In this case, we compute the average with the moving average formula:

$$f_t(a_1) \leftarrow f_t(a_1) + \frac{a_2 - f_t(a_1)}{\#_t(a_1)}, \quad (1)$$

where $\#_t(a_1)$ is the number of times we tried to add an entry with key a_1 to the map f_t . Note that consequently we have to keep track of $\#_t(a_1)$, i.e., we have to annotate each entry of the map with the corresponding cardinality.

Training Step 1-3 are done for all T1W/T2W scan pairs available in the training data set, and the values found in Step 3 are always inserted into the same tables. So we get as many tables as we have macro clusters, and up to as many rows as we have micro clusters for *all* training images. Since we process many scans, the full tables get too large, and in reality, we only store a meaningful subset of the rows. When querying for a T2W, we can compute missing values by interpolation.

What is left to describe is how we now synthesize images based on our mapping tables. We implemented two options (the second one is faster).

Synthesizing T2W: For a patient whose T2W is missing, we preprocess the T1W scan and then cluster it with k -means1d to obtain a macro clustering. We load all tables f_t into the memory which were computed with the same number of macro clusters. Let t be one of the macro clusters. We consider each point p belonging to cluster t . We find the two rows of f_t with the closest intensity values to p and interpolate $f_t(p)$ from these two rows. The resulting intensities form a synthesized scan. Once it is computed, it is postprocessed using a 3×3 median filter [7] to remove *salt-and-pepper* noise which was present in the synthesized images.

Synthesizing T2W in Search Mode: We noticed that having large tables computed by training on many images (e.g., 200) produces noise in the results. Thus, we propose an additional method that does not precompute a large model before querying, but instead computes a small model every time we want to answer a query, which we call *Search*. Given a T1W query image, we first search in the training data set for the w patients whose T1W has the smallest mean squared error to the query T1W (where w is a small constant, e.g. $w = 5$). Then, we create a small model by performing the training process only on these w patients, and produce the synthesized T2W with this model. This approach has the downside that we have to create a new model for every single query, thus significantly increasing the query time. However, since we choose small values for w , a synthesized T2W image for one input can be computed in around ten minutes, without the need of computing a model beforehand.

We compare the classic Train&Test mode and Search mode with $w \in \{5, 10\}$ and using 3, 4, 5 and 6 macro clusters, for a total of 12 different models.

3 Pix2Pix

Pix2Pix [14, 34] is a general solution to the pixel-to-pixel translation problem. Given an input image and an output image, this neural network framework is able to learn a relationship between the two. At inference time, it applies the learned function to create a new, previously unseen image. Pix2Pix is based on *conditional GANs* (cGAN) [22]. A cGAN is a neural network framework that simultaneously trains two models, a *generator* G and a *discriminator* D , which engage in an adversarial process. During training, the generator starts with random noise as input, aiming to produce data resembling the training set. The discriminator evaluates the generated data, providing feedback to adjust the generator’s parameters. Simultaneously, the discriminator learns to better distinguish between real and generated data, refining its parameters to maximize correct classifications.

The Pix2Pix objective function is a fusion between the traditional cGAN loss [22] and the L1 loss. We build our objective function by further expanding this concept. Let G and D be any non-linear

mapping functions and let x, y represent our input and our desired output respectively. The generator is asked to learn the distribution of the data y from noise z such that it represents a mapping from a given input x , i.e., $G : \{x, z\} \rightarrow y$. The discriminator with mapping $D(y)$ outputs the probability that y comes from the training data. In fact, we train D to maximize the probability that the real data y is identified as real, while we train G to maximize the probability that the data generated from noise $G(z)$ is detected as real by the discriminator. The latter objective corresponds to minimizing $1 - D(G(z))$. The final form of Equation (2) below comes from formalizing these high-level objectives with the log-loss principle of multi-class classification problems. Additionally, Isola et al. [14] add the term (3), which means that the objective of the discriminator is unchanged, whereas the generator is asked to trick the discriminator while maintaining a small loss. Since our objective is to have a low mean squared error in the tumor area, such that tumors can be easily identified, we added (4) to the loss function. T is a matrix that is zero where there is no tumor and one otherwise, \odot is the Hadamard product and $\text{sum}(T)$ is the grand sum of the matrix T , i.e., the number of tumor voxels. Our loss function is

$$= \mathbb{E}_{x,y} [\log D(x, y)] + \mathbb{E}_{x,z} [\log(1 - D(x, G(x, z)))] \quad (2)$$

$$+ \lambda \cdot \mathbb{E}_{x,y,z} [\|y - G(x, z)\|_1] \quad (3)$$

$$+ \gamma \cdot \mathbb{E}_{x,y,z} \left[\frac{1}{\text{sum}(T)} \cdot \|T \odot y - G(T \odot x, T \odot z)\|_2^2 \right]. \quad (4)$$

As it is usual in machine learning, the best values for λ and γ can be found with a hyperparameter optimization.

Additionally, we implement some other modifications: 1) We modify the loading functionality to accept three-dimensional NIfTI images. 2) We extend the data augmentation process with an additional library, TorchIO [27], which implements useful preprocessing and data augmentation routines for medical imaging. 3) We add the mixed precision training functionality from NVIDIA APEX (available at <https://github.com/NVIDIA/apex>). Operations like matrix to matrix multiplication and convolution are then performed in half-precision floating-point format, which results in a speed-up at training time. 4) Since a big portion of our scans is background, the L1 loss is only computed on the actual brain voxels. 5) Recent studies have shown that the transpose convolution operation during upsampling creates checkerboard artifacts [24, 35]. We implement the solution of Wojna et al. [35]: *linear additive upsampling*. This method has been successfully used for the generator of Pix2PixHD [34] and applied on CT scans [11]. We substitute the transpose convolution operation with a two-factor upsampling followed by a 4-factor reduction of the number of channels, and finally by a 3×3 convolution with stride 1. We use bilinear upsampling if the scans are two-dimensional, and trilinear upsampling for the three-dimensional case.

The default generator architecture for Pix2Pix is a UNet [31], more specifically a UNet-256, which requires an input with side length multiple of 256. Given the 3D nature of the scans and the increased memory usage, we opt for a UNet-128 model with seven downsampling and seven upsampling blocks. During training, the images are preprocessed to have side length 128 by performing random crops, while during inference they are padded to have side length 256. Additional augmentation is done by randomly flipping the images. We also test whether ResNets [12], which are used by Pix2PixHD [34], are a better choice for our model. We apply the Adam solver [17] with a learning rate of 0.0002, the momentum parameters $\beta_1 = 0.5, \beta_2 = 0.999$ and a batch size of 1. All other network parameters are the default ones given by Pix2Pix. We train 16 models per generator architecture (UNet or ResNet) with the values $\lambda, \gamma \in \{0, 100, 500, 1000\}$ for a total of 32 different models.

4 Experimental Evaluation

We test BrainClustering and Pix2Pix. As baseline, we use the complementary approach described in Section 1 and a simple method that we name Random, which consists of filling all non-background voxels by uniformly distributed random values.

Table 1: Our split into data sets of the BraTS 19 data.

Data set	N. Patients	Segmentation
	N. Patients	Ground Truth
<code>training</code>	270	BraTS 19
<code>validation</code>	30	BraTS 19
<code>testBraTS</code>	35	BraTS 19
<code>testOUR</code>	15	anonymous
<code>no-ground-truth</code>	110	/

4.1 Data

Our collective contains a total of 460 patients from BraTS 19 [2, 3, 21]. Each patient has four three-dimensional MRI brain scans (T1W, T2W, T1CE, FLAIR) of size (240, 240, 155) in NIfTI (*Neuroimaging Informatics Technology Initiative*) format. All scans have been preprocessed to have the same voxel size (1mm³), are skull-stripped and registered to the same anatomical template. A ground truth segmentation that shows the exact position of the tumor is present for 350 patients have. Most of the tumor ground truth comes from BraTS, and a portion of the scans has been manually segmented by a radiologist from the University Hospital of Cologne (C.Z.) and the segmentation has later been converted to the BraTS labels. A detailed representation of the BraTS 19 tumor labels is given by Bakas et al. [2]. Each voxel is identified as either background (no tumor), non-enhancing part of the tumor and necrotic core, excess of fluid associated with the tumor (edema), or contrast enhanced part of the tumor.

We divide the data into a training set, a validation set, and three test sets (Table 1). The training set is used to train both approaches, the validation set to optimize the hyperparameters, and the three test sets to evaluate the approaches. We evaluate `testBraTS` and `testOUR` separately due to the different sources of ground truth.

4.2 Code and System

BrainClustering is written in C++17 and ported to Python with Boost.Python [6], while our Pix2Pix implementation is written in Python3.8 and uses the machine learning framework PyTorch [26]. Our implementations are available at <https://github.com/giuliabaldini/brainclustering> and <https://github.com/giuliabaldini/Pix2PixNIfTI>. The BrainClustering scans are produced using a computer cluster with 36 nodes and two Intel Xeon CPU E5-2690 v2 CPUs per node with 10 cores each and 128 GB of RAM. We compute the Pix2Pix scans, the segmentation and the evaluation results on a machine with eight 32 GB NVIDIA Tesla V100-SXM2.

4.3 Evaluation Methods

We evaluate:

a) *Visual Similarity to Real Scans*, evaluated by computing *Average Mean Squared Errors* (MSEs) to the original scans. We compute the MSE between the real T2W and each synthesized T2W in the brain mask voxels and, if the tumor ground truth is available, we additionally compute the MSE restricted to the tumor area. Finally, we normalize all values to [0, 1].

b) *Usefulness for Segmentation*: We use a DeepMedic [16] model to evaluate the usefulness of the synthesized images for segmentation. The model was computed on the `training` data set with all four MRI scans and the corresponding tumor ground truth as input. The hyper parameters were chosen according to a clinical evaluation on DeepMedic [28]. The model is trained to predict three tumor classes: necrotic/non-enhancing tumor, edema and contrast enhanced tumor.

For the evaluation, we compute the segmentation with the DeepMedic model on the test data sets using the synthesized T2W (instead of the real T2W scan) and the real T1W, T1CE and FLAIR. We use Dice scores [5] and undirected 95th Hausdorff distance [32] (HD95) as evaluation metrics. For the case of `testBraTS` and `testOUR`, we compute the Dice score and the HD95 between the segmentation

produced with the synthesized images and the ground truth segmentation. For **no-ground-truth**, these values are computed in comparison to the segmentation produced with the real T2W (instead of the ground truth segmentation). Following the BraTS evaluation [2, 3, 21], we assess the tumor classes based on three categories: whole tumor (necrotic/non-enhancing tumor, edema and contrast enhanced tumor), tumor core (necrotic/non-enhancing tumor and contrast enhanced tumor), and active tumor (contrast-enhanced tumor) and then compute the average of the three cases.

5 Results

Figure 3 up to Figure 5 give a visual impression of the resulting synthesized images for the **testOUR** data set. In Figure 3, we present two synthesized images produced by BrainClustering and Pix2Pix for two patients. The second and fourth row show the segmentation achieved by using the respective image as T2W. The rightmost image in the “Real T1W” column shows the ground truth image and segmentation. Figure 4 and Figure 5 present the middle transversal slice for each MRI in **testOUR** with the segmentation superimposed on the scans.

5.1 Run Time

BrainClustering Train&Test takes 2.2 hours on average to train on 270 patients, and testing takes around 9 seconds per scan. By comparison, Search 5 and Search 10 take respectively 2.5 minutes and 4.8 minutes per patient. The Pix2Pix ResNet training takes around 9 hours, while the Pix2Pix UNet training takes around 3 hours. The testing process takes around 7 seconds per scan. The baseline methods can be computed in negligible time since only one pass over T1W is required for Complementary and Random can be computed without looking at the input data.

5.2 Mean Squared Error Evaluation

In Figure 6, we present the MSE results for the **testBraTS**, **testOUR** and **no-ground-truth** data sets. To improve clarity, we have selected two BrainClustering, two Pix2Pix ResNet and two Pix2Pix UNet models, which are those that performed best on the validation data set in the respective category. Random has been excluded from the figure because its MSEs are too large (averaging at 0.37 on the brain mask and 0.11 on the brain tumor area). The second baseline, Complementary evaluates to reasonable MSEs, e.g., it has 0.04 on average in the brain mask and 0.03 in the tumor area on **testBraTS**. All our methods improve upon these values as can be seen in Figure 6. The scans generated by Pix2Pix have a better MSE than BrainClustering in the brain mask area. In the tumor area, the average MSE of both methods is comparable, and it is overall better, although the median MSE is still below 0.02. The best results are produced by Pix2Pix ResNet with $\lambda = 500$ and $\gamma = 500$, but Pix2Pix UNet with $\lambda = 100$ and $\gamma = 0$ also produces good results. Notably, BrainClustering with Search with 10 patients and 5 clusters achieves the best median MSE in the tumor area among all methods we tested. We conclude that it is possible to compute synthesized scans that closely resemble the true scan.

5.3 Segmentation Evaluation

Figure 7 shows the segmentation results for the same models. All our methods perform better than Complementary, and Pix2Pix performs better than BrainClustering. For Pix2Pix, the ResNet models are in most cases better than the UNet ones. The segmentations with the original T2W obtain an average Dice score of 0.833 on **testOUR** and of 0.748 on **testBraTS**, and an average of 0.774 for both data sets together. The overall best performing Pix2Pix approach is with $\lambda = 100$ and $\gamma = 0$, with an average Dice of 0.807 on **testOUR** and of 0.744 on **testBraTS**, and an average of 0.763 for both data sets together. For BrainClustering, the best method is Search with 10 scans, 5 macro clusters and 100 micro clusters, with an average Dice of 0.741 on **testOUR** and of 0.739 on **testBraTS**, and an average of 0.739 for both data sets together. This method achieves an average HD95 of 12.047 on **testOUR**, of 8.021 on **testBraTS** and of 9.229 for both data sets together. On **no-ground-truth**, the best Pix2Pix model achieved a Dice score of 0.858 and an HD95 of 4.706 and the best BrainClustering model achieved a Dice score of 0.794 and an HD95 of 6.213.

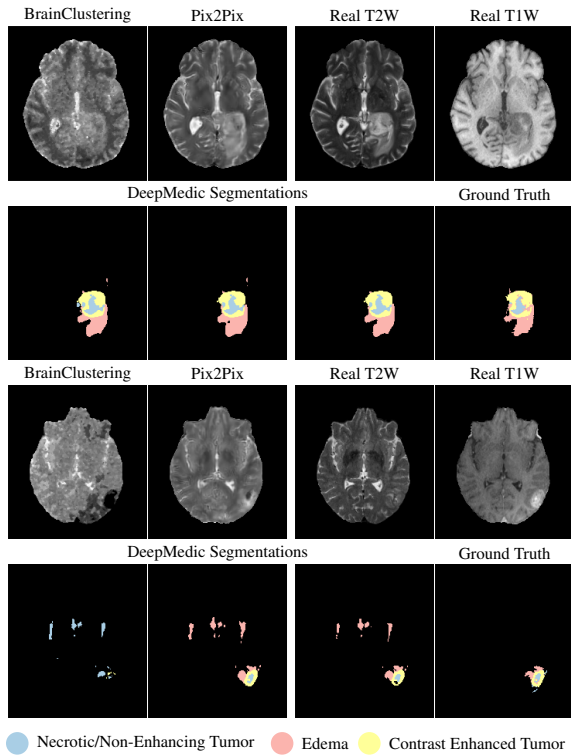


Figure 3: The segmentations in the second and in the fourth row have been created using the respective T2W and the three original T1W, T1CE, FLAIR. The rightmost image in the “Real T1W” column shows the real T1W image and the ground truth segmentation.

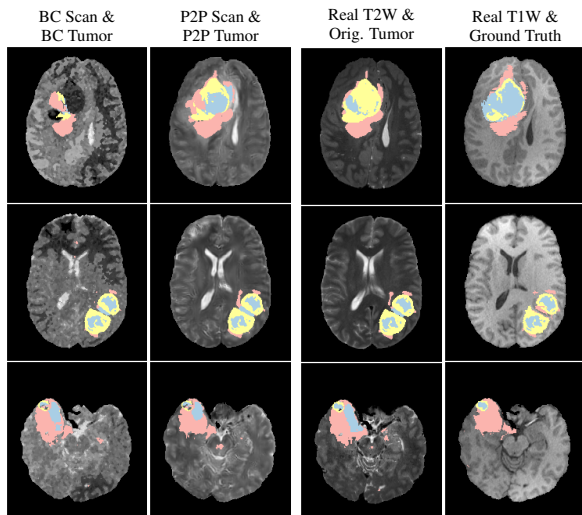


Figure 4: BrainClustering, Pix2Pix and original T2W scans and corresponding superimposed segmentation generated with DeepMedic (together with the real T1W, T1CE and FLAIR), shown for all cases from the `testOUR` data set. In the last column the ground truth segmentation is superimposed on the T1W scan.

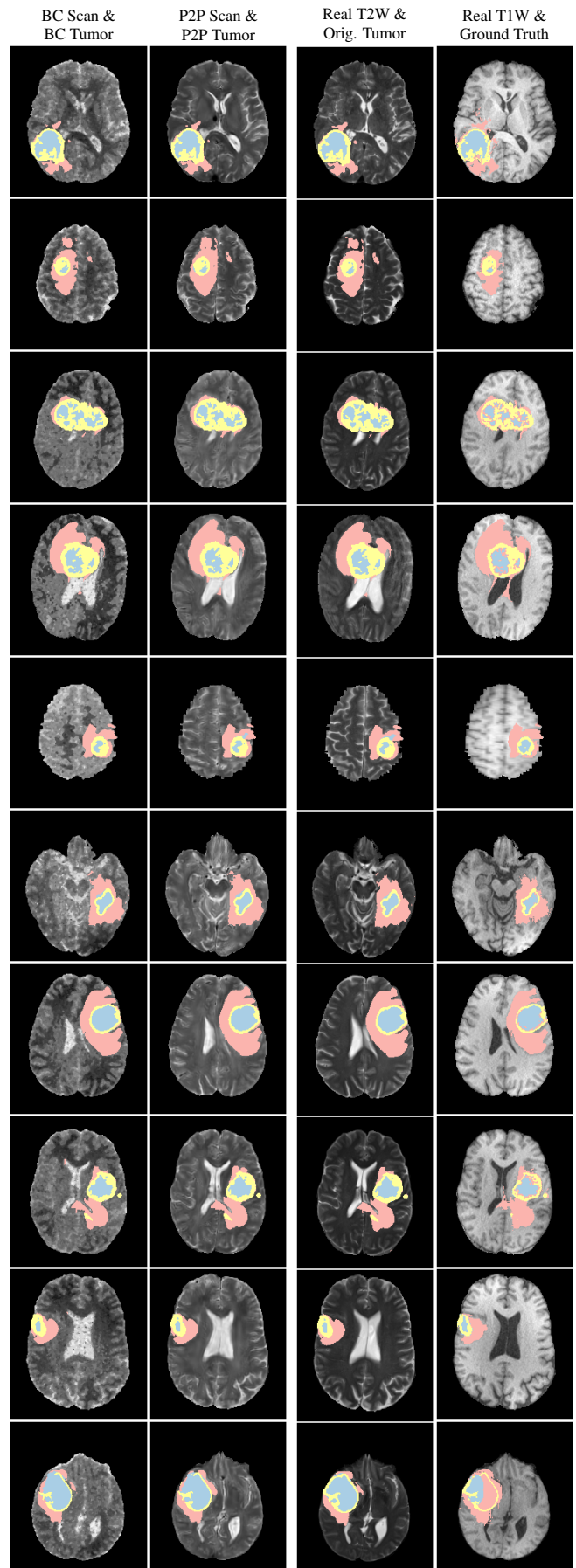


Figure 5: Continuation of Figure 4.

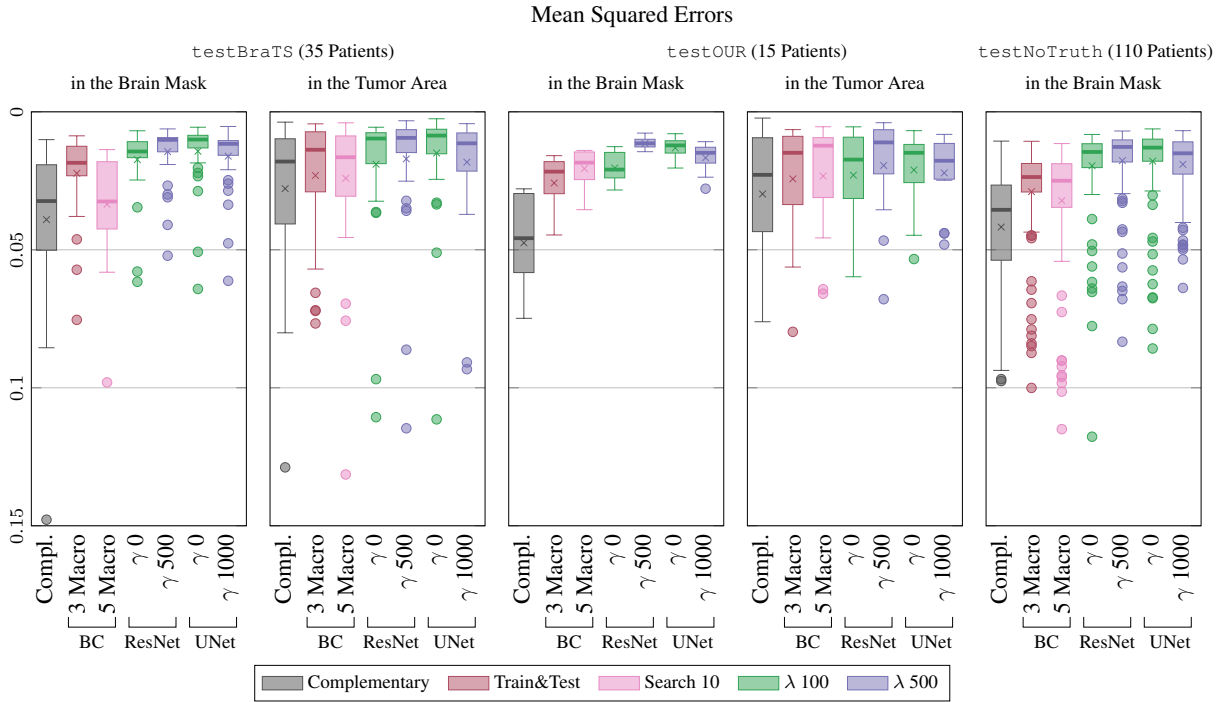


Figure 6: [Best viewed in color] Comparison of different approaches with respect to MSE in the brain mask and (if available) in the tumor areas. The scores represent the distribution of the patients. A lower value indicates a better score. The crosses represent the averages, the thick bars are the medians and the dots are the outliers.

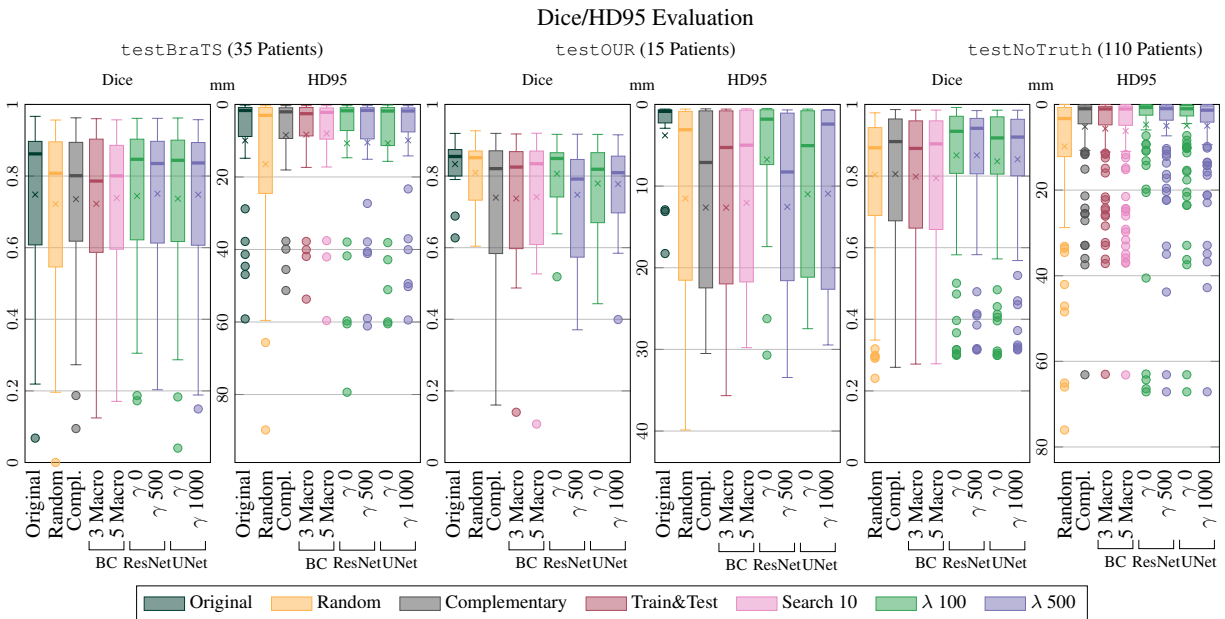


Figure 7: [Best viewed in color] Comparison with respect to the true tumor segmentation (for `testBraTS` and `testOUR`) and the original tumor segmentation (for `testNoTruth`) using Dice and undirected 95th Hausdorff distance (HD95). For `testBraTS` and `testOUR`, we also include the segmentation which is produced by using the real T2W as *Original* to give a positive baseline as to what scores are achievable if T2W was reproduced perfectly. We compute the Dice score and the undirected 95% percent Hausdorff distance on three different regions and average the scores. The box plots represent the distribution of the patients. For the Dice score a higher value indicates a better value whereas for the Hausdorff distance the opposite holds. The crosses represent the averages, whereas the thick bars are the means and the dots are the outliers.

So note that for the data set with ground truth (`testOUR` and `testBraTS`), the best performing Pix2Pix method leads to an average Dice score of 0.763 compared to an average score of 0.774 when using the real T2-weighted, so it is very close (BrainClustering performs a bit worse, achieving an average score of 0.739). As an additional overview, Table 2 shows the difference in the metrics when

Table 2: Mean and standard deviation of (Method-Dice - Original-Dice) and (Original-HD95 - Method-HD95). Negative values indicate a decrease in quality.

Approach	<code>testBraTS</code>	<code>testOUR</code>
Average Change in Dice Score		
Random	-0.0267 ± 0.0839	-0.0242 ± 0.0693
Complementary	-0.0129 ± 0.0904	-0.0936 ± 0.1729
BC Train/3 Macro	-0.0258 ± 0.0738	-0.0960 ± 0.1830
BC-S 10/5 Macro	-0.0097 ± 0.1002	-0.0920 ± 0.1862
ResNet 100/0	-0.0038 ± 0.0561	-0.0268 ± 0.0757
ResNet 500/500	$+0.0024 \pm 0.0584$	-0.0857 ± 0.1271
UNet 100/0	-0.0115 ± 0.0579	-0.0541 ± 0.0927
UNet 500/1000	-0.0003 ± 0.0546	-0.0558 ± 0.1024
Average Change in 95% Hausdorff Distance		
Random	-6.5477 ± 12.7633	-7.7170 ± 10.9374
Complementary	$+1.4568 \pm 11.1163$	-8.8377 ± 10.3483
BC Train/3 Macro	$+1.6263 \pm 11.5007$	-8.8494 ± 11.0154
BC-S 10/5 Macro	$+1.9030 \pm 10.5994$	-8.2579 ± 10.1501
ResNet 100/0	-0.7786 ± 7.4124	-2.9560 ± 7.9400
ResNet 500/500	-0.5746 ± 5.7906	-8.7538 ± 9.7339
UNet 100/0	-0.7717 ± 5.4584	-7.1996 ± 9.1900
UNet 500/1000	$+0.0282 \pm 4.4942$	-7.1382 ± 10.5381

replacing the real T2W by a synthesized T2W scan. The Pix2Pix ResNet approach with $\lambda = 100$ and $\gamma = 0$ decreases the Dice score by less than 0.01 on `testBraTS`, and by less than 0.03 on `testOUR`. The average Dice score of the original segmentations on `testBraTS` and `testOUR` are 0.748 and 0.833, so the average decreases in Dice score are below 1% and 4% of the original score.

An interesting byproduct of our work is that we observe that substituting the T2W image with random noise also produced acceptable results. This is a common practice that gets some justification from our evaluation. However, the best tested methods outperform this workaround.

5.4 Concluding remarks

A general limitation of trying to reproduce a missing scan is that if something is only visible in the missing scan, then obviously it cannot be synthesized. However, our study shows that in many cases, enough information is contained in T1W and a useful synthesized T2W can be computed. The BrainClustering pictures are sometimes noisy but achieve a low average MSE. The Pix2Pix pictures are a bit too light, but capture the structure very well. The segmentation is often only mildly or not at all affected by replacing the real T2W by synthesized ones. The proposed methods can thus aid already trained segmentation networks whenever the T2W modality is missing.

References

- [1] Hazem Abdelmotaal, Ahmed A Abdou, Ahmed F Omar, Dalia Mohamed El-Sebaity, and Khaled Abdelazeem. “Pix2pix conditional generative adversarial networks for Scheimpflug camera color-coded corneal tomography image generation”. en. In: *Transl. Vis. Sci. Technol.* 10.7 (June 2021), p. 21 (cit. on p. 2).

- [2] Spyridon Bakas, Hamed Akbari, Aristeidis Sotiras, Michel Bilello, Martin Rozycki, et al. “Advancing The Cancer Genome Atlas glioma MRI collections with expert segmentation labels and radiomic features”. In: *Scientific Data* 4.170117 (Sept. 2017). DOI: 10.1038/sdata.2017.117 (cit. on pp. 2, 6, 7).
- [3] Spyridon Bakas, Mauricio Reyes, Andras Jakab, Stefan Bauer, Markus Rempfler, et al. *Identifying the Best Machine Learning Algorithms for Brain Tumor Segmentation, Progression Assessment, and Overall Survival Prediction in the BraTS Challenge*. arXiv:1811.02629. 2018. URL: <https://arxiv.org/abs/1811.02629> (cit. on pp. 2, 6, 7).
- [4] Farideh Bazangani, Frédéric J P Richard, Badih Ghattas, Eric Guedj, and Alzheimer’s Disease Neuroimaging Initiative. “FDG-PET to T1 weighted MRI translation with 3D Elicit generative adversarial network (E-GAN)”. en. In: *Sensors (Basel)* 22.12 (June 2022), p. 4640 (cit. on p. 2).
- [5] Jeroen Bertels, Tom Eelbode, Maxim Berman, Dirk Vandermeulen, Frederik Maes, et al. “Optimizing the Dice Score and Jaccard Index for Medical Image Segmentation: Theory & Practice”. In: *CoRR* abs/1911.01685 (2019). arXiv: 1911.01685. URL: <http://arxiv.org/abs/1911.01685> (cit. on p. 6).
- [6] *Boost.Python*. https://www.boost.org/doc/libs/1_75_0/libs/python/doc/html/index.html. Accessed: 2023-08-06 (cit. on p. 6).
- [7] G. Bradski. *The OpenCV Library*. Dr. Dobb’s Journal of Software Tools. 2000. URL: <https://opencv.org/> (cit. on p. 4).
- [8] L. Caldeira, P. Almeida, and J. Seabra. “MR Brain Tumor Segmentation using Clustering”. In: *Proc. ESMRMB Congress*. Antalya, Turkey, Sept. 2009, pp. 48–49. DOI: 10.1007/s10334-009-0175-1 (cit. on p. 2).
- [9] H. Al-Dmour and A. Al-Ani. “MR Brain Image Segmentation Based on Unsupervised and Semi-Supervised Fuzzy Clustering Methods”. In: *Proc. IEEE DICTA*. Gold Coast, QLD, Australia, Nov. 2016, pp. 1–7. DOI: 10.1109/DICTA.2016.7797066 (cit. on p. 2).
- [10] Allan Grønlund, Kasper Green Larsen, Alexander Mathiasen, Jesper Sindahl Nielsen, Stefan Schneider, et al. *Fast Exact k-Means, k-Medians and Bregman Divergence Clustering in 1D*. arXiv:1701.07204. 2018. URL: <http://arxiv.org/abs/1701.07204> (cit. on p. 3).
- [11] J. Haubold, R. Hosch, L. Umutlu, A. Wetter, P. Haubold, et al. “Contrast agent dose reduction in computed tomography with deep learning using a conditional generative adversarial network”. In: *Eur. Radiol.* (Feb. 2021). DOI: 10.1007/s00330-021-07714-2 (cit. on pp. 2, 5).
- [12] Kaiming He, Xiangyu Zhang, Shaoqing Ren, and Jian Sun. *Deep Residual Learning for Image Recognition*. arXiv:1512.03385. 2015. URL: <https://arxiv.org/abs/1512.03385> (cit. on p. 5).
- [13] Fabian Isensee, Paul F. Jaeger, Simon A. A. Kohl, Jens Petersen, and Klaus H. Maier-Hein. “nnU-Net: a self-configuring method for deep learning-based biomedical image segmentation”. In: *Nat. Methods* 18 (Dec. 2020), pp. 203–211. DOI: 10.1038/s41592-020-01008-z (cit. on p. 1).
- [14] Phillip Isola, Jun-Yan Zhu, Tinghui Zhou, and Alexei A. Efros. “Image-to-Image Translation with Conditional Adversarial Networks”. In: *Proc. IEEE CVPR*. Honolulu, HI, USA, July 2017, pp. 5967–5976. DOI: 10.1109/CVPR.2017.632 (cit. on pp. 1, 2, 4, 5).
- [15] R. Jonker and A. Volgenant. “A Shortest Augmenting Path Algorithm for Dense and Sparse Linear Assignment Problems”. In: *Computing* 38 (Dec. 1987), pp. 325–340. DOI: 10.1007/BF02278710 (cit. on p. 3).
- [16] Konstantinos Kamnitsas, Christian Ledig, Virginia F. J. Newcombe, Joanna P. Simpson, Andrew D. Kane, et al. “Efficient Multi-Scale 3D CNN with Fully Connected CRF for Accurate Brain Lesion Segmentation”. In: *Medical Image Analysis* 36 (Mar. 2016), pp. 61–78. DOI: 10.1016/j.media.2016.10.004 (cit. on pp. 1, 6).
- [17] Diederik P. Kingma and Jimmy Ba. *Adam: A Method for Stochastic Optimization*. arXiv:1412.6980. 2017. URL: <https://arxiv.org/abs/1412.6980> (cit. on p. 5).

- [18] Hongwei Bran Li, Gian Marco Conte, Syed Muhammad Anwar, Florian Kofler, Koen Van Leemput, et al. “The Brain Tumor Segmentation (BraTS) Challenge 2023: Brain MR Image Synthesis for Tumor Segmentation (BraSyn)”. In: *CoRR* abs/2305.09011 (2023). DOI: 10.48550/arXiv.2305.09011. arXiv: 2305.09011. URL: <https://doi.org/10.48550/arXiv.2305.09011> (cit. on p. 2).
- [19] Mingjiang Li, Jincheng Zhou, Dan Wang, Peng Peng, and Yezhao Yu. “Application of clustering-based analysis in MRI brain tissue segmentation”. en. In: *Comput. Math. Methods Med.* 2022 (Aug. 2022), p. 7401184 (cit. on p. 2).
- [20] M. Malathi and P. Sinthia. “MRI Brain Tumour Segmentation Using Hybrid Clustering and Classification by Back Propagation Algorithm”. In: *Asian Pacific journal of cancer prevention* 19.11 (Nov. 2018), pp. 3257–3263. DOI: 10.31557/APJCP.2018.19.11.3257 (cit. on p. 2).
- [21] Bjoern H. Menze, Andras Jakab, Stefan Bauer, Jayashree Kalpathy-Cramer, Keyvan Farahani, et al. “The Multimodal Brain Tumor Image Segmentation Benchmark (BRATS)”. In: *IEEE Transactions on Medical Imaging* 34.10 (10 Oct. 2015), pp. 1993–2024. DOI: 10.1109/TMI.2014.2377694 (cit. on pp. 2, 6, 7).
- [22] Mehdi Mirza and Simon Osindero. *Conditional Generative Adversarial Nets*. arXiv:1411.1784. 2014. URL: <http://arxiv.org/abs/1411.1784> (cit. on p. 4).
- [23] G. Mirzaei and H. Adeli. “Segmentation and clustering in brain MRI imaging”. In: *Reviews in the Neurosciences* 30.1 (Sept. 2018), pp. 31–44. DOI: 10.1515/revneuro-2018-0050 (cit. on p. 2).
- [24] Augustus Odena, Vincent Dumoulin, and Chris Olah. “Deconvolution and Checkerboard Artifacts”. In: *Distill* (2016). DOI: 10.23915/distill.00003 (cit. on p. 5).
- [25] Thiagarajan Padmapriya, Padmanaban Sriramakrishnan, Thiruvenkadam Kalaiselvi, and Karuppanagounder Somasundaram. “Advancements of MRI-based brain tumor segmentation from traditional to recent trends: A review”. en. In: *Curr. Med. Imaging Rev.* 18.12 (2022), pp. 1261–1275 (cit. on p. 1).
- [26] Adam Paszke, Sam Gross, Francisco Massa, Adam Lerer, James Bradbury, et al. “PyTorch: An Imperative Style, High-Performance Deep Learning Library”. In: *CoRR* abs/1912.01703 (2019). arXiv: 1912.01703. URL: <http://arxiv.org/abs/1912.01703> (cit. on p. 6).
- [27] Fernando Pérez-García, Rachel Sparks, and Sebastien Ourselin. *TorchIO: a Python library for efficient loading, preprocessing, augmentation and patch-based sampling of medical images in deep learning*. arXiv:2003.04696. 2020. URL: <http://arxiv.org/abs/2003.04696> (cit. on p. 5).
- [28] Michael Perkuhn, Pantelis Stavrinou, Frank Thiele, Georgy Shakirin, Manoj Mohan, et al. “Clinical Evaluation of a Multiparametric Deep Learning Model for Glioblastoma Segmentation Using Heterogeneous Magnetic Resonance Imaging Data From Clinical Routine”. In: *Invest. Radiol.* 53.11 (Nov. 2018), pp. 647–654. DOI: 10.1097/RLI.0000000000000484 (cit. on p. 6).
- [29] Ramin Ranjbarzadeh, Annalina Caputo, Erfan Babae Tirkolae, Saeid Jafarzadeh Ghouschi, and Malika Bendeche. “Brain tumor segmentation of MRI images: A comprehensive review on the application of artificial intelligence tools”. en. In: *Comput. Biol. Med.* 152.106405 (Jan. 2023), p. 106405 (cit. on p. 1).
- [30] P. Raut, G. Baldini, M. Schöneck, and L. Caldeira. “Using a generative adversarial network to generate synthetic MRI images for multi-class automatic segmentation of brain tumors”. In: *Frontiers in Radiology* 3 (2024). ISSN: 2673-8740. DOI: 10.3389/fradi.2023.1336902 (cit. on p. 2).
- [31] Olaf Ronneberger, Philipp Fischer, and Thomas Brox. *U-Net: Convolutional Networks for Biomedical Image Segmentation*. arXiv:1505.04597. 2015. URL: <https://arxiv.org/abs/1505.04597> (cit. on p. 5).
- [32] Greg Sharp, Ziji Wu, Marta Peroni, Justin Lee, Rui Li, et al. *Plastimatch*. 2011. URL: <http://plastimatch.org/> (cit. on p. 6).
- [33] Daniel Steinberg. *kmeans1d*. 2020. URL: <https://github.com/dstein64/kmeans1d> (cit. on p. 3).

- [34] Ting-Chun Wang, Ming-Yu Liu, Jun-Yan Zhu, Andrew Tao, Jan Kautz, et al. “High-Resolution Image Synthesis and Semantic Manipulation with Conditional GANs”. In: *Proc. IEEE CVPR*. Salt Lake City, UT, USA, June 2018, pp. 8798–8807. DOI: 10.1109/CVPR.2018.00917 (cit. on pp. 2, 4, 5).
- [35] Zbigniew Wojna, Vittorio Ferrari, Sergio Guadarrama, Nathan Silberman, Liang-Chieh Chen, et al. *The Devil is in the Decoder: Classification, Regression and GANs*. arXiv:1707.05847. 2019. URL: <https://arxiv.org/abs/1707.05847> (cit. on p. 5).
- [36] Xiaolin Wu. “Optimal Quantization by Matrix Searching”. In: *J. Algorithms* 12 (4 Dec. 1991), pp. 663–673. DOI: 10.1016/0196-6774(91)90039-2 (cit. on p. 3).
- [37] Bingbao Yan, Miao Cao, Weifang Gong, and Benzheng Wei. “Multi-scale brain tumor segmentation combined with deep supervision”. en. In: *Int. J. Comput. Assist. Radiol. Surg.* 17.3 (Mar. 2022), pp. 561–568 (cit. on p. 1).
- [38] Qianye Yang, Nannan Li, Zixu Zhao, Xingyu Fan, Eric I-Chao Chang, et al. “MRI cross-modality image-to-image translation”. en. In: *Sci. Rep.* 10.1 (Feb. 2020), p. 3753 (cit. on p. 2).